Aalto University

OPEN ACCESS

This is an electronic reprint of the original article.
This reprint may differ from the original in pagination and typographic detail.

Rontu, Ville; Nolvi, Anton; Hokkanen, Ari; Haeggstrom, Edward; Kassamakov, Ivan; Franssila, Sami

Elastic and fracture properties of free-standing amorphous ALD Al2O3 thin films measured with bulge test

Published in:
Materials Research Express

DOI:
10.1088/2053-1591/aabbd5

Published: 01/04/2018

Document Version
Peer-reviewed accepted author manuscript, also known as Final accepted manuscript or Post-print

Published under the following license:
CC BY

Please cite the original version:
Rontu, V., Nolvi, A., Hokkanen, A., Haeggstrom, E., Kassamakov, I., & Franssila, S. (2018). Elastic and fracture properties of free-standing amorphous ALD Al2O3 thin films measured with bulge test. *Materials Research Express*, *5*(4), Article 046411. https://doi.org/10.1088/2053-1591/aabbd5

This material is protected by copyright and other intellectual property rights, and duplication or sale of all or part of any of the repository collections is not permitted, except that material may be duplicated by you for your research use or educational purposes in electronic or print form. You must obtain permission for any other use. Electronic or print copies may not be offered, whether for sale or otherwise to anyone who is not an authorised user.

Elastic and fracture properties of free-standing amorphous ALD Al_2O_3 thin films measured with bulge test

Ville Rontu[1], Anton Nolvi[2,3], Ari Hokkanen[1], Edward Haeggström[2], Ivan Kassamakov[2,4] and Sami Franssila[1]

1 Aalto University, Department of Chemistry and Materials Science, and Micronova Centre for Nanofabrication, P. O. Box 13500, FIN-00076, Aalto, Espoo, Finland

2 University of Helsinki, Department of Physics, Helsinki, Finland

3 Åbo Akademi University, Faculty of Science and Engineering, Pharmaceutical Sciences Laboratory, Turku, Finland

4 University of Helsinki, Helsinki Institute of Physics, Helsinki, Finland

E-mail: ville.rontu@aalto.fi

Abstract. We have investigated elastic and fracture properties of amorphous Al_2O_3 thin films deposited by atomic layer deposition (ALD) with bulge test technique using a free-standing thin film membrane and extended applicability of bulge test technique. Elastic modulus was determined to be 115 GPa for a 50-nm thick film and 170 GPa for a 15-nm thick film. Residual stress was 142 MPa in the 50-nm Al_2O_3 film while it was 116 MPa in the 15-nm Al_2O_3 film. Density was 3.11 g/cm^3 for the 50-nm film and 3.28 g/cm^3 for the 15-nm film. Fracture strength at 100 hPa/s pressure ramp rate was 1.72 GPa for the 50-nm film while for the 15-nm film it was 4.21 GPa, almost 2.5-fold. Fracture strength was observed to be positively strain-rate dependent. Weibull moduli of these films were very high being around 50. The effective volume of a circular film in bulge test was determined from a FEM model enabling future comparison of fracture strength data between different techniques.

1. Introduction

Designing and modelling microelectromechanical system (MEMS) devices require information about thin film material properties, as opposed to bulk material properties. Preferably, these properties are measured from test specimens that resemble the actual devices, by methods that mimic the actual operating environment. Sample processing for instance may alter the material properties significantly [1]. Scale dependency of material properties is well known and usually taken into account. Strain-rate dependent fracture strength demonstrates yet another peculiarity for the material testing: the specimen might withstand high strain-rate shocks, but rupture unexpectedly when subject to a low strain-rate.

FEM-modelling can be used to predict the mechanical behavior of a MEMS device at the design stage if the proper material properties are used. These models, however, cannot usually predict the failure of the device, which is why experimental data on the fracture properties is important.

Bulge test [2–6] is a suitable method to measure thin film elastic properties such as elastic modulus, residual stress and fracture strength. In a bulge test, a free-standing membrane that is fixed from the edges is loaded from one side by a fluid. This type of testing resembles the operating environment of many membrane devices like pressure sensors, microphones, x-ray windows, thermopile detectors and microhotplates.

Atomic layer deposition (ALD) has been established as the deposition method for applications, which require uniform and precise layer thicknesses. ALD films can be continuous and pin-hole free already at one nanometer thickness [7]. Al_2O_3 is the most commonly applied ALD film and it is used as a model case for ALD film growth [8, 9]. Still, there is room to improve in the understanding of its mechanical properties. Ylivaara et al. reported [10] a thorough investigation on the elastic properties of ALD Al_2O_3 measuring elastic modulus, hardness and residual stress for a wide range of film thicknesses and growth temperatures. Gaskins et al. also recently reviewed mechanical properties of ALD Al_2O_3 among other properties [11]. Elastic modulus of ALD Al_2O_3 is in the range of 140–180 GPa for films deposited in temperatures from 100–300 °C [10, 11]. Spread in the elastic modulus is mostly associated with density of the deposited films. Films with lower density have smaller elastic modulus. Especially with lower deposition temperatures, a clear drop in the density and elastic modulus is observed corresponding with increase in hydrogen content in the films [10]. All as-deposited ALD Al_2O_3 films in this temperature range have resulted in amorphous microstructure. The elastic modulus of ALD Al_2O_3 is comparable to amorphous Al_2O_3 obtained with other methods such as sputtering [12, 13] and evaporation [14]. Consistently it has been observed that the elastic modulus of amorphous Al_2O_3 is less than a half of the elastic modulus for bulk crystalline Al_2O_3 (450 GPa single crystalline α-Al_2O_3 [14], 415 GPa polycrystalline α-Al_2O_3 [15]). Even though these studies have been quite thorough, fracture properties of amorphous ALD Al_2O_3 have been studied only on few occasions [5, 6, 16, 17]. On polymer substrates, Jen et al. [17] observed increase in critical strains for onset of film cracking with decreasing film thicknesses. Critical tensile strains increased from 0.5 % at 80 nm film thickness to 2.4 % at 5 nm. We previously determined with bulge test method the fracture strength of 70 nm thick ALD Al_2O_3 membranes to be 2.25–3 GPa [5, 6]. However, we have not studied scale nor scale nor strain-rate dependency of the elastic and fracture properties. In this research, the elastic and fracture properties of free-standing ALD Al_2O_3 thin films of two different thicknesses (15 and 50 nm) is measured with the bulge test using two different loading schemes (constant pressure ramp-up rate and stepwise pressure increase). As a result, strain-rate dependent fracture strength is observed.

2. Methods

2.1. Sample fabrication

Free-standing circular membranes (diaphragm) of 400-µm diameter on 7x7-mm^2 chips were fabricated on 100-mm double-side polished (100) silicon wafers by ALD Al_2O_3 deposition, lithography, wet etching in buffered hydrofluoric acid (BHF) and deep reactive ion etching (DRIE). Al_2O_3 was deposited simultaneously on both sides of the silicon wafer from trimethylaluminum ($AlMe_3$) and H_2O in Beneq TFS500 reactor at 300 °C temperature and 1 hPa pressure. The precursors were kept at a room temperature and vapor drawn into the reactor. Target thicknesses were 15 and 50 nm and the number of deposition cycles 150 and 500, respectively. One cycle consists of 0.2 s $AlMe_3$ pulse, followed by 1 s wait time after closing pulsing valve and 1 s purge with N_2, and 0.2 s H_2O pulse, followed by 0.75 s wait time and 1 s purge. Thickness was measured after deposition by Plasmos SD2300 HeNe single wavelength ellipsometer and later verified by x-ray reflection (XRR). Density of the layers was determined from the XRR using a Rigaku Smartlab X-ray diffractometer. After the Al_2O_3 deposition, the wafer front side was protected with a resist and a lithography on the backside determined the 400-µm diameter holes and the 100-µm wide dicing lines. The Al_2O_3 on the backside was etched in buffered hydrofluoric acid (BHF) at a room temperature after which all resist was stripped. The sample wafer was glued to a carrier wafer using photoresist to prevent chip detachment when the through-wafer etching was complete. The DRIE etching was done with a Bosch process in a STS ASE tool with a SF_6 and O_2 etching chemistry and a C_4F_8 passivation chemistry using the Al_2O_3 as a hard mask. The selectivity between Al_2O_3 and Si has been measured to be 1:100000 in a Bosch process [18]. Finally, the separated chips were detached from the carrier wafer in acetone and cleaned with oxygen plasma.

2.2. Bulge testing

Bulge testing was performed using two different set-ups. The first bulge test set-up had a scanning white light interferometer (SWLI) allowing measurement of the displacement as a function of the pressure. A more detailed description of the custom-built SWLI can be found in ref. [19] and about the bulge setup in ref. [5]. This set-up was used to measure the pressure-displacement curves from which the elastic modulus and the residual stress was determined. The pressure was increased stepwise by manually adjusting pressure regulator (Aga 600B 7P) attached to the argon bottle. Displacement of the membrane was measured with SWLI only when the pressure in the gas lines had saturated. The pressure was measured using a precision digital pressure manometer (Huber Instrumente HM35) attached to the gas line and applied to the chip from the backside.

The samples were attached to blocks of polydimethylsiloxane (PDMS) (Sylgard 184) which had a hole punched through to apply pressure. The attachment was done by applying uncured PDMS around the edges of the membrane chip. Following this, the samples were cured in an oven at 60 °C for 30 minutes. The PDMS on top and underneath of the membrane chip ensured pressure tight clamping with the aluminum holder.

The elastic modulus, E, and the residual stress, σ_0, were extracted from the pressure-displacement curve by fitting an analytical expression for the pressure P as a function of the membrane deflection, d,

$$P(d) = C_1 \frac{h\sigma_0}{a^2} d + C_2 f(v) \frac{E}{(1-v)} \frac{h}{a^4} d^3 \quad (1)$$

to the pressure-displacement curve [20]. In the equation (1) h is the membrane thickness, a is the membrane diameter and v is the Poisson's ratio, which is assumed to be 0.24 for amorphous Al_2O_3 [21, 22]. The coefficients $C_1 = 4$, $C_2 = 2.67$ and $f(v) = (1.026 + 0.233v)^{-1}$ were determined from FEM results by Pan et al. [20] for circular films.

The second bulge test set-up was used to measure the fracture strength. It had a computer controlled pressure regulator enabling programmed ramp rates. In the measurements, the pressure was applied from the top and a 100 hPa/s ramp rate was used until a fracture was observed. 30–35 membranes of both thicknesses were measured to reach statistically significant sample size [23, 24].

According to Beams [2], the stress, σ, at the top of a bulge that is shaped as a hemispherical cap can be approximated with a relation

$$\sigma = \frac{Pa^2}{4hd} \quad (2)$$

and the strain, ε, with

$$\epsilon = \frac{2d^2}{3a^2}. \quad (3)$$

The total stress can also be described with the Hooke's law relating the stress due to the stretching and the initial stress as

$$\sigma = \frac{E}{1-v}\epsilon + \sigma_0. \quad (4)$$

By solving (2) for the membrane deflection d, substituting it into (3) and finally inserting into (4) yields a third degree polynomial

$$\sigma^3 - \sigma_0\sigma^2 - \frac{1}{24}\frac{EP^2a^2}{(1-v)h^2} = 0, \quad (5)$$

from which the total stress can be solved by finding the real root.

Similarly, an equation for the strain can be obtained by solving (3) for the d, substituting it into (2) and inserting into (4). This yields

$$\frac{E^2}{(1-v)^2}\epsilon^3 + \frac{2\sigma_0 E}{1-v}\epsilon^2 + \sigma_0^2\epsilon - \frac{1}{24}\frac{P^2a^2}{h^2} = 0. \quad (6)$$

The residual stress terms in (5) and (6) become significant at small deflections or large residual stresses. A tensile residual stress gives the membrane flexural rigidity, which the thin membrane would otherwise lack.

Fracture strength, σ_f, is calculated from the rupture pressure, P_{max}, by using the equation (5). Weibull analysis is performed for the fracture strength data. Cumulative distribution function of a multimodal Weibull distribution is described as a weighted sum of individual distributions [25]

$$F_{1,..,S}(\sigma_f) = 1 - \sum_{i=1}^{S} p_i \, e^{-\left(\frac{\sigma_f}{\sigma_{\theta i}}\right)^{m_i}} \qquad \sum_{i=1}^{S} p_i = 1, \tag{7}$$

where p_i is the portion of components in a subpopulation i (for unimodal distribution ($S = 1$), $p_1 = 1$), m is a shape parameter known as the Weibull modulus and σ_θ characteristic strength corresponding to the stress level with a 63.2 % probability of failure. The characteristic strength is related to the Weibull material scale parameter σ_0, which has units GPa·$(m^3)^{1/m_V}$, by the expression

$$\sigma_\theta = \sigma_0 V_{eff}^{-1/m_V} \text{ [23].} \tag{8}$$

V_{eff} is the effective volume, which for a uniaxial tension equals the sample volume V and for other loading configurations is less than V. The V_{eff} can be calculated from

$$V_{eff} = \int_V \left(\frac{\sigma}{\sigma_{max}}\right)^{m_V} dV \text{ [23].} \tag{9}$$

Either a unimodal ($S = 1$) or a bimodal ($S = 2$) Weibull distribution is used to extract the performance data. The bimodal distribution reduces from 6- to 5-parameter distribution from the fact that $p_2 = 1 - p_1$. The bimodal Weibull distribution takes into account two separate subpopulations of defects resulting in the failure. The existence of two or more different subpopulations is evident if the fracture strength data in the Weibull plot does not fall into a straight line. Distribution fitting is performed in the Matlab® using the maximum likelihood estimate (MLE) method.

Mean σ_M of the Weibull distribution is given by

$$\sigma_M = \sigma_\theta \left[\Gamma\left(1 + \frac{1}{m}\right)\right], \tag{10}$$

where $\Gamma(x)$ is the gamma function. Standard deviation is given by

$$s = \sqrt{\sigma_\theta^2 \left[\Gamma\left(1 + \frac{2}{m}\right) - (\Gamma\left(1 + \frac{1}{m}\right))^2\right]}. \tag{11}$$

2.3. Modeling

Free-standing ALD membranes were modeled with the finite element method (FEM) using a Comsol Multiphysics software. We used a structural mechanical model with an axisymmetric geometry and a stationary solver. Circular 50-nm thick and 450-µm diameter membrane was modelled as an ideal case.

In the model, silicon (Si) chip has also a circular shape because of the axisymmetric geometry. A three-dimensional model with a real square shape silicon chip is also possible, but axisymmetric geometry has a denser calculation mesh, which produces results that are more accurate. The chip size is significantly larger than the membrane size so the chip can be approximated as circular. The calculation mesh for the 50-nm thick film used for effective volume calculations consisted of 500000 square 5x5-nm elements. The FEM model used Al_2O_3 density of 3100 kg/m^3, elastic modulus of 112 GPa and residual stress of 127 MPa for the 50-nm thick membrane. The material parameters of the Si part were from the Comsol's material library for an isotropic single crystal Si: density 2329 kg/m^3, elastic modulus 170 GPa and Poisson's ratio 0.28.

In order to validate experimental results circular 450-µm diameter Al_2O_3 membranes were modelled with 48.1 and 14.8 nm thickness. The 48.1-nm and the 14.8-nm membranes calculation mesh contained 20000 and 50000 elements, respectively. The FEM model used the densities measured with XRR for 48.1-nm thick film and 14.8-nm thick membrane, and the elastic modulus and the residual stress calculated from experimental results. The stress and deflection were modeled in a pressure range from 50–1000 hPa.

3. Results

3.1. Sample fabrication

Thickness and density of the Al_2O_3 film was measured by XRR. The thickness was 48.1±1 nm for 500 cycles and 14.8±1 nm for 150 cycles. This corresponds to growth per cycle of 0.97 Å, which is in accordance with literature [10]. The density was 3.11±0.1 g/cm^3 for 48.1-nm thick film and 3.28±0.1 g/cm^3 14.8-nm thick film. Density for ALD Al_2O_3 grown at 300 °C is commonly observed to be around 3.1–3.2 g/cm^3 [10, 26]. Uniformity was better than ±1 nm as determined by ellipsometer from five points across the wafer.

Diameter of the window opening was much larger than the design value of 400 µm. This resulted from widening in the DRIE through-wafer etch step. The actual diameter of each membrane was measured individually from optical microscope images and the resulting values were used in the calculations. The diameters varied from 438–508 µm for 48.1-nm thick membranes and 428–460 µm for 14.8-nm membranes. The reason for the widening of the hole from the diameter defined by the lithography and the spread in the diameters are due to a combination of negative tapering of the side walls, non-uniformity in the etch rate and notching effect [27].

3.2. Elastic modulus and residual stress

In order to determine the elastic modulus and the residual stress, the deflection was measured with a SWLI as a function of the applied pressure. The whole membrane area was scanned and the silicon surface was kept as the reference surface for the deflection. This eliminates the possible bulging of the sample holder. The measurement was performed with discrete pressure steps because each SWLI scan

took a few minutes. Before each scan, the pressure and the deflection were allowed to stabilize. Figure 1 shows the pressure-deflection behavior of a 48.1-nm thick Al_2O_3 membrane measured three times. In the first and the second run, the pressure was released prior to the film rupture. The overlapping pressure deflection data for the subsequent measurements demonstrate that the deformation is fully elastic. This also means that no delamination of the film occurred. The film was driven to rupture on the third loading. For the 48.1-nm thick membranes the rupture occurred in a 470–570 hPa range whereas for 14.8-nm thick membranes in a 190–390 hPa range.

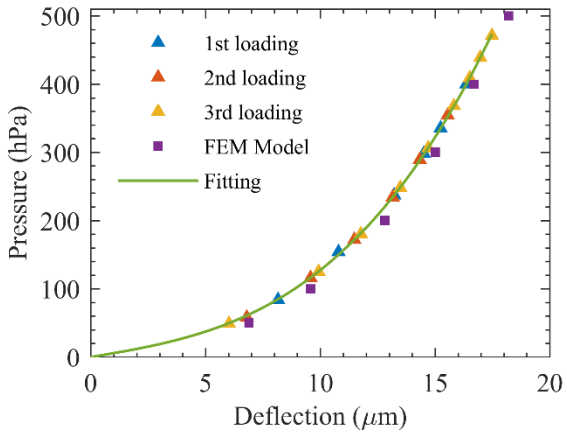

Figure 1. Pressure-deflection behavior on three successive loadings of 48.1-nm thick 450-µm diameter Al_2O_3 membrane. Fitting of the Eq. (1) yielded values of 115 GPa for E and 151 MPa for σ_0. The results from a FEM model using the extracted values are shown for comparison.

Fitting of the equation (1) into the pressure-deflection data (shown for a single sample in figure 1) yielded average value of 115±3 GPa for E and 142±22 MPa for σ_0 for the 48.1-nm thick Al_2O_3 films. For the 14.8-nm thick Al_2O_3 films average value of 177±5 GPa for E and 116±20 MPa for σ_0 were obtained. The elastic modulus of 48.1-nm thick film is low compared to literature whereas the elastic modulus of the thinner film compares well with literature value of 165–180 GPa for films deposited at 300 °C [10]. The magnitude of residual stress is slightly lower compared to literature value of 180 MPa [10]. It seems that the elastic modulus increases as the thickness decreases, while the residual stress remains unchanged. However, it was also noticed that the 48.1-nm film had a slightly lower density compared to the 14.8-nm film and the lower elastic modulus could be related to the lower film density.

3.3. Fracture strength

With a constant pressure ramp rate, the strain rate is not constant. Instead, the strain rate decreases non-linearly as shown in figure 2. The strain rate is calculated by differentiating strain calculated with equation (6) for time for a 100 hPa/s ramp rate. The strain rate is on the order of 10^{-3} to 10^{-4} s^{-1}, which is typical for tensile tests [28].

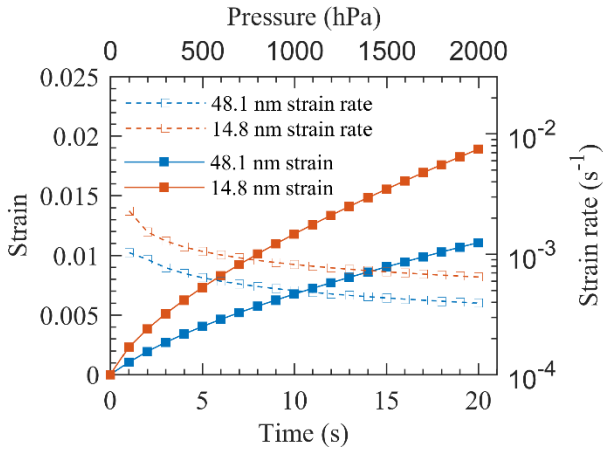

Figure 2. The strain and the strain rate at a 100 hPa/s ramp rate for a 450-µm diameter membrane.

The average rupture pressure was 1750±190 hPa for the 48.1-nm thick membranes and 1810±90 hPa for the 14.8-nm thick membranes at a 100 hPa/s pressure ramp rate. These are significantly higher values than what we observed for the samples in the stepwise pressure ramp test (470–570 hPa and 190–390 hPa for 48.1-nm and 14.8-nm thick membranes, respectively). It seems also that at a higher pressure ramp rate, the thinner membranes are relatively more pressure tolerant than the thicker membranes, which is the opposite to what was observed when measuring the pressure-deflection curves at discrete pressure steps. The rupture pressures correspond to critical strain of 1 % and 1.8 % according to equation (6) for 48.1-nm and 14.8-nm thick films respectively, which is in close agreement with critical tensile strains for onset of cracking observed on polymer substrates [17].

Fracture strength was calculated from the rupture pressure according to the equation (5) and fitted into the Weibull distribution in the equation (7). Figure 3 shows the Weibull probability plots for the 48.1-nm thick and the 14.8-nm thick Al_2O_3 membranes. The 48.1-nm thick membranes had a clear shoulder on the Weibull probability plot in dictating that a bimodal Weibull distribution would better describe the data set. Bimodality in the fracture strength indicates that a single population of defects is not responsible for all the failures [23, 24]. Here the subpopulation with a lower fracture strength is thought to consist of surface defects originating from the fabrication process. The 14.8-nm thick membranes had only one outlier and a unimodal Weibull distribution described it the best. The mean and the standard deviation were calculated from the equations (10) and (11) respectively. The mean fracture strength for 48.1-nm thick Al_2O_3 membranes was 1.72±0.04 GPa and for 14.8-nm thick membranes 4.21±0.10 GPa. Previously we observed fracture strength of 3.1 GPa for 75 nm thick Al_2O_3 membranes [6]. However, the Weibull modulus, m, for the 75 nm thick Al_2O_3 membranes was only 15 whereas we now observe m around 50 for both 14.8 and 48.1 nm thick Al_2O_3 membranes.

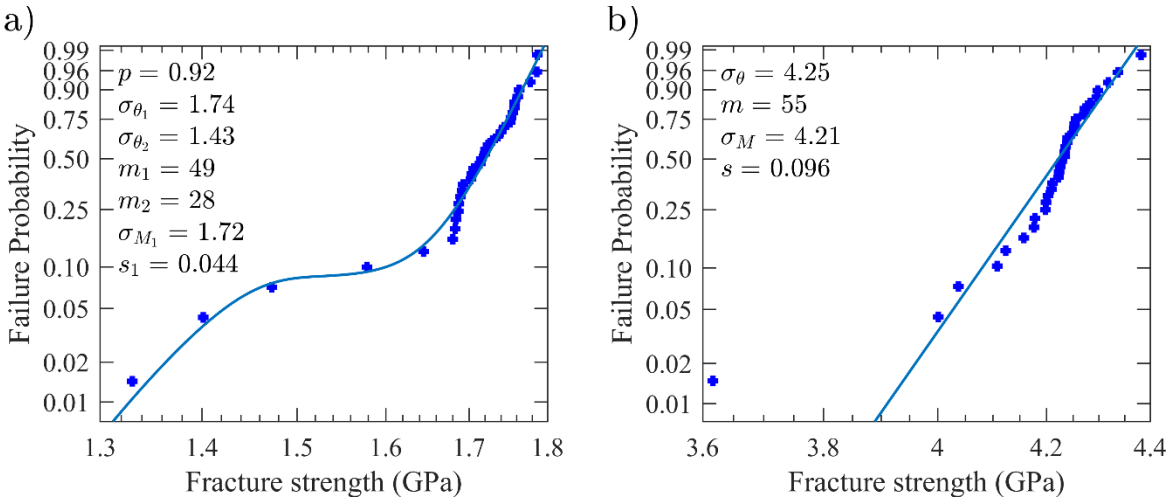

Figure 3. Weibull probability plots for the 48.1-nm (a)) and 14.8-nm thick (b)) Al_2O_3 membranes. The Weibull probability function was fitted with two subpopulations on the left and with a single subpopulation on the right.

The effective volume of a bulge test was calculated according to the equation (9) from the stress field obtained from a FEM model. When calculating the effective volume, the stress maximum was assumed to occur at the center of the membrane. The stress field was cut off 1 µm before Si edge to remove stress artefacts from the film/silicon interface (see section 3.4. for more details). The effective volume varies only as a function of the Weibull modulus for a given loading geometry. Figure 4 shows the ratio V_{eff}/V as a function of Weibull modulus m. The fitting follows

$$\frac{V}{V_{eff}} = \frac{15}{\sqrt{m^2 + 92m + 179}}, \tag{12}$$

from which it is possible to calculate the effective volume in a bulge test at any value of m for a circular membrane.

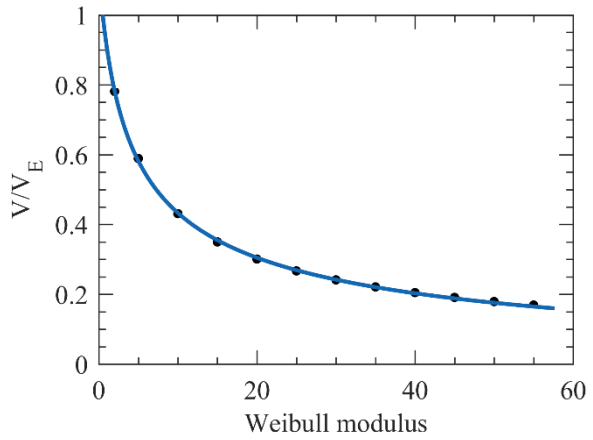

Figure 4. The ratio of the effective volume to the volume as a function of the Weibull modulus for the bulge test of circular membrane.

From the effective volume, the Weibull modulus and the characteristic strength, extraction of the Weibull material scale parameter σ_0 is possible according to the equation (8). For the 48.1-nm thick films σ_{01} is 0.87 GPa·$(m^3)^{(1/49)}$ and for the 14.8-nm thick films 2.23 GPa·$(m^3)^{(1/55)}$.

3.4. Modeling

The highest stress values were calculated to locate at the edge of the free-standing membrane, where the bulk silicon is removed by the DRIE etching. In Figure 5, a 50-nm membrane with a 225-µm radius is loaded by 500-hPa differential pressure. The maximum stress value is 5.17 GPa at the edge of the film and 5.41 GPa on the silicon, whereas in the middle of the membrane the stress value was only 0.79 GPa at the same pressure level. The stress maximum at the edge is likely an artefact from the edge constraints in the model and is strongly dependent on the mesh size. A finer mesh, as seen in figure 5, pinpoints the stress maximum to the interface between the Si and the Al_2O_3 film. A general assumption is that the stress maximum of the film occurs in the middle of the membrane and that the fracture occurs there. The ultimate tensile strength was calculated by us as the maximum tensile stress at the center of the membrane at the pressure when the film ruptured. The stress and the deflection of the 48.1-nm and 14.8-nm thick membrane at a 1000-hPa differential pressure are shown in figure 6.

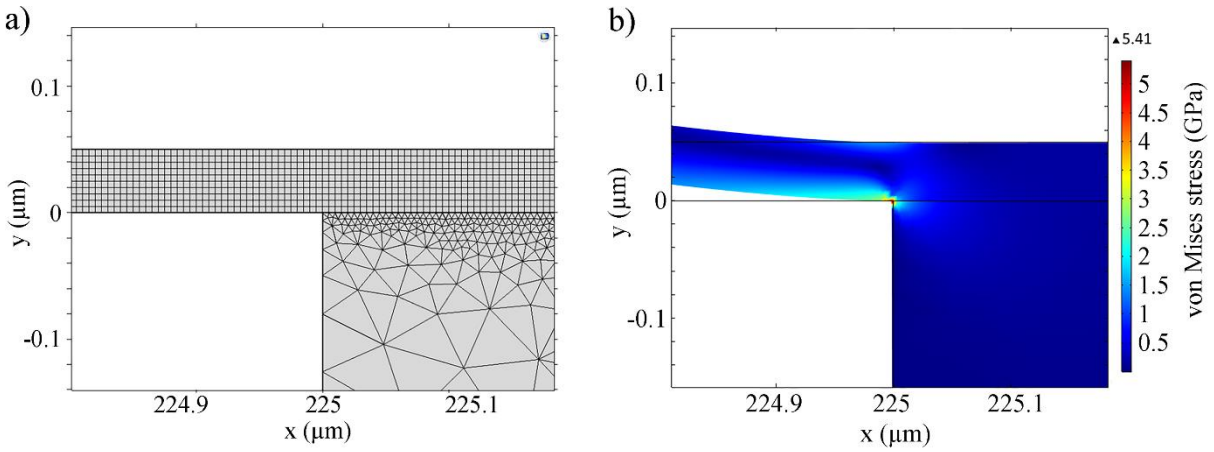

Figure 5. The calculation mesh used in the FEM model (a)) and the stress at the edge of a circular membrane loaded with a 500-hPa differential pressure (b)).

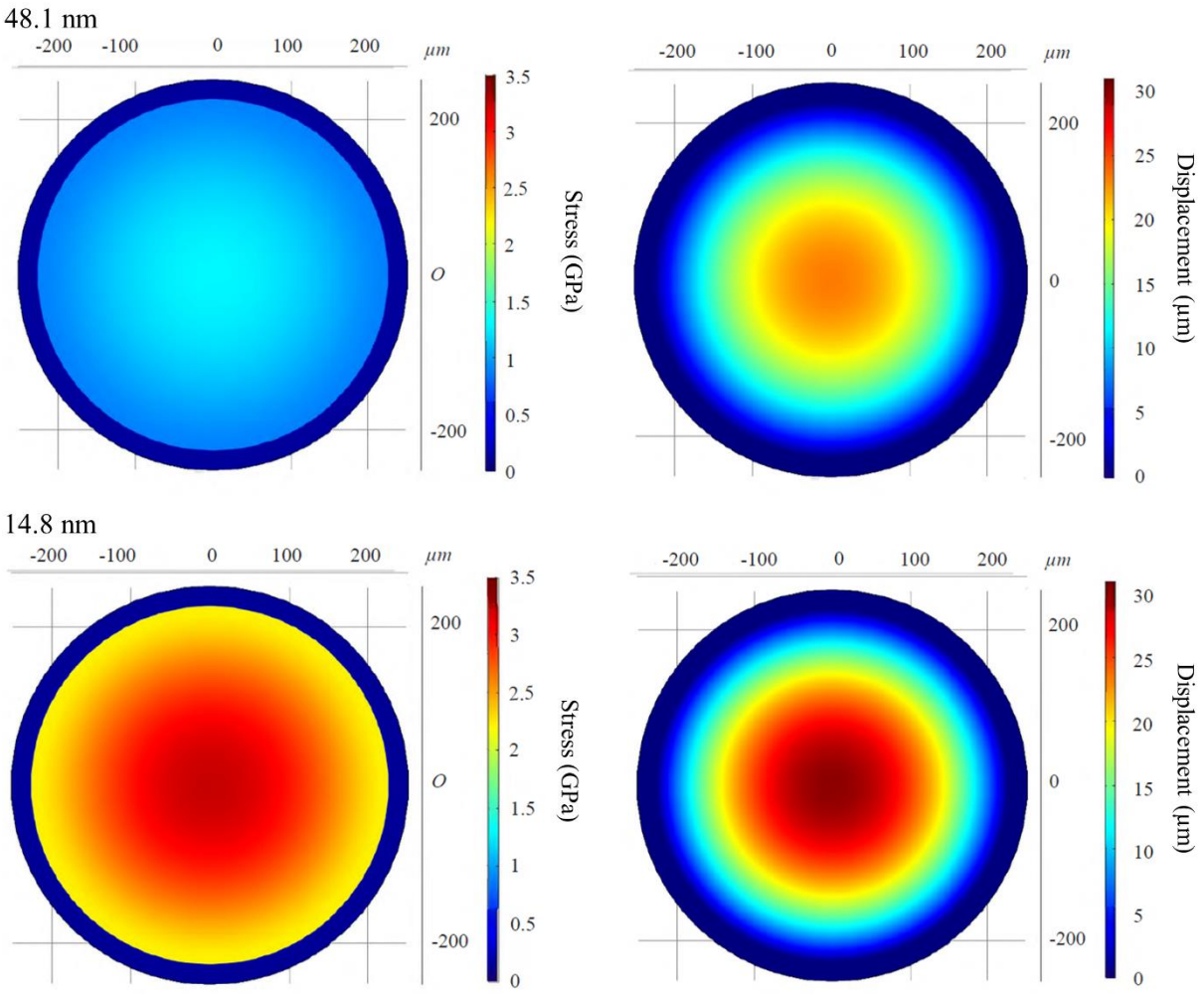

Figure 6. The stress and the deflection of a 48.1-nm and a 14.8-nm thick membrane at a 1000-hPa pressure differential over the membrane.

4. Discussion

The mechanical properties of the Al_2O_3 membranes that we measured are comparable to what has been previously measured [5, 6, 10, 29]. The elastic modulus of our 48.1-nm thick film is low, but there is a noticeable increase in the elastic modulus for the thinner film. The thinner film's elastic modulus is similar (177 GPa vs. 165–175 GPa) to what was measured with nanoindentation and laser-generated surface acoustic waves (LSAW) by Ylivaara et al. [10] for films grown at 300 °C. Ylivaara et al. did not notice an increase in elastic modulus with a decreasing film thickness nor a difference in the densities of films of different thickness. The density of the 48.1-nm thick film is similar to Ylivaara et al. results (3.11 g/cm^3), but our thinner film appears more dense (3.28 g/cm^3). This might also explain the difference in elastic modulus and fracture strength between the films. Previously it has been observed that less dense films have lower elastic modulus [10, 11]. However, it is not known why the thinner film is denser. It could be that the hydrogen content in the films is different as it is associated

with density [10]. The difference could come from some variation in the process conditions. However, no abnormalities were observed during deposition.

The residual stress of our films was slightly lower (120–140 MPa vs. 180 MPa) than what Ylivaara et al. [10] observed for films deposited at 300 °C. However, Ylivaara et al. calculated the film stress from the wafer curvature, which describes approximately the average stress over the wafer whereas the bulge test is a more localized method. In addition, when the film is released some stress relaxation might occur. The difference between the residual stress values for our 14.8-nm and 48.1-nm thick films is within the error margins and there appears to be no thickness dependence on the residual stress, which is in accordance to previous studies [10].

The mean fracture strength for the 48.1-nm thick membranes was lower than what we reported previously in [6] for 75-nm thick membranes (1.5 GPa vs. 3.1 GPa), even though smaller volumes should result in a higher fracture strength. Both of the films were deposited at 300 °C, although on a different ALD tool, and measured with the same pressure ramp rate. However, the films in [6] had a higher elastic modulus than our 48.1-nm thick film. If we calculate the mean fracture strength for a 75-nm thick and 400-μm diameter membrane using the equation (8) and the material parameters obtained for our 14.8-nm thick film, we reach an expected mean fracture strength of 4.1 GPa. This value is higher than obtained in [6] and not much different from the fracture strength of our 14.8-nm film because of the very high Weibull modulus measured for our films. Weibull moduli that we have now measured for both 48.1-nm and 14.8-nm thick films are much higher than what was measured previously for 75-nm films (49 and 55 versus 15)[6].

The pressure tolerance and the increase of the fracture strength for the thinner membranes are noticeable. The 14.8-nm thick membranes withstood similar pressures as the 48.1-nm thick membranes when the pressure ramp rate was 100 mbar/s, leading to the very high fracture strength values. However, when the pressure ramp was performed incrementally the pressure tolerance decreased. In our pressure-deflection data, a single measurement took tens of minutes as the pressure was increased incrementally and a SWLI scan was performed only when the deflection and the pressure had stabilized. This led to a film rupture already below 600 hPa for the 48.1-nm thick membranes and below 400 hPa for the 14.8-nm thick membranes. Positive dependency of fracture strength on the strain rate has been reported in literature for amorphous silica glass in molecular dynamics models [30, 31] and experimentally [32, 33]. It is possible that The huge difference in the fracture strength that we have observed is significant and affects the applicability of the aluminum oxide films in MEMS devices.

5. Conclusions

Bulge test is a valid method to determine the mechanical and the fracture properties for free-standing thin films. The ratio of effective volume to volume was determined for circular films in the bulge test

as a function of Weibull modulus, which enables deduction of the Weibull material scale parameter and comparison of the fracture strength data to data measured with other methods.

Further research is required to understand the origin of fracture. Such a test could be made for example by using a high-speed camera to monitor the film deflection and breakage. The FEM-model pinpoints the maximum stress to the film/substrate interface, which constitute below 0.1 % of the membrane volume. If this stress is true and the film fracture initiates from the boundary, all the fracture strength measurements done so far are invalid as the film rupture and the maximum stress have been assumed to locate at the center of the film.

The fracture strength of amorphous Al_2O_3 thin films is observed to be positively strain-rate dependent. However, further experiments are required to understand the extent of the strain-rate dependency and the mechanism for strain-rate sensitivity.

The applicability of amorphous Al_2O_3 films in MEMS devices is still limited by the lack of understanding in the elastic and the fracture properties. Deeper understanding is required in order to design reliable devices.

Acknowledgments

Authors would like to acknowledge Micronova Nanofabrication Centre of Aalto University for providing facilities for the sample fabrication. Mr. Jouni Heino from Helsinki Institute of Physics is thanked for assistance in the bulge measurements. V. R. is grateful for funding from the Finnish Cultural Foundation. The work was partly funded by the TEKES project Superwindows.

References

[1] Chen K.-S., Ayon A. and Spearing S. M. 2000 Controlling and testing fracture strength of silicon on the mesoscale J. Am. Ceram. Soc. **83** 1476–1484

[2] Beams J. W. 1959 Mechanical properties of thin films of gold and silver Structure and properties of thin films, Wiley, New York, 183–192

[3] Vlassak J. J., Nix W. D. 1992 A new bulge test technique for the determination of Young's modulus and Poisson's ratio of thin films J. Mater. Res. **7** 3242–3249

[4] Edwards R. L., Coles G., Sharpe, Jr W. N. 2004 Comparison of tensile and bulge tests for thin-film silicon nitride Exp. Mech. **44** 49–54

[5] Berdova M., Ylitalo T., Kassamakov I., Heino J., Törmä P. T., Kilpi L., Ronkainen H., Koskinen J., Haeggström E. and Franssila S. 2014 Mechanical assesment of suspended ALD thin films by bulge and shaft-loading techniques Acta Mater. **66** 370–377

[6] Berdova M., Ylivaara O. M. E., Rontu V., Törmä P. T., Puurunen R. L. and Franssila S. 2015 Fracture properties of atomic layer deposited aluminum oxide free-standing membranes J. Vac. Sci. Technol., A **33** 01A106

[7] Grigoras K., Sainiemi L., Tiilikainen J., Säynätjoki A., Airaksinen V.-M., Franssila S. 2007 Application of ultra-thin aluminum oxide etch mask made by atomic layer deposition technique J. Phys.: Conf. Ser. **61** 369–373

[8] Puurunen R. L. 2005 Surface chemistry of atomic layer deposition: a case study for the trimethylaluminum/water process J. Appl. Phys. **97** 121301

[9] George S. M. 2010 Atomic layer deposition: an overview Chem. Rev. **110** 111–131

[10] Ylivaara O. M. E. et al. 2014 Aluminum oxide from trimethylaluminum and water by atomic layer deposition: the temperature dependence of residual stress, elastic modulus, hardness and adhesion Thin Solid Films **552** 124–135

[11] Gaskins J. T. et al. 2017 Review—Investigation and review of the thermal, mechanical, electrical, optical, and structural properties of atomic layer deposited high-k dielectrics: beryllium oxide, aluminum oxide, hafnium oxide, and aluminum nitride ECS J. Solid State Sci. Technol. **10** N189–N208

[12] Koski K., Hölsä J., Juliet P. 1999 Properties of aluminium oxide thin films deposited by reactive magnetron sputtering Thin Solid Films **339** 240–248

[13] Hughey M. P., Cook R. F., Thurn J. 2005 Stress stability and thermo-mechanical properties of reactively sputtered alumina films J. Mater. Sci. **40** 6345–6355

[14] Chechenin N. G., Bøttiger J., Krog J. P. 1997 Nanoindentation of amorphous aluminum oxide films III. The influence of the substrate on the elastic properties Thin Solid Films **304** 70–77

[15] Munro R. G. 1997 Evaluated material properties for sintered α-alumina J. Am. Ceram. Soc. **80** 1919–1928

[16] Miller D. C. et al. 2009 The mechanical robustness of atomic-layer- and molecular-layer-deposited coatings on polymer substrates J. Appl. Phys. **105** 093527

[17] Jen S.-H., Bertrand J. A., George S. M. 2011 Critical tensile and compressive strains for cracking of Al_2O_3 films grown by atomic layer deposition J. Appl. Phys. **109** 084305

[18] Dekker J., Kolari K., Puurunen R. L. 2006 Inductively coupled plasma etching of amorphous Al_2O_3 and TiO_2 mask layers grown by atomic layer deposition J. Vac. Sci. Technol., B **24** 2350–2355

[19] Kassamakov I., Seppänen H. O., Oinonen M. J., Hæggström E. O., Österberg J. M., Aaltonen J. P., Saarikko H., Radivojevic Z. P. 2007 Scanning white light interferometry in quality control of single-point tape automated bonding Microelectron. Eng. **84** 114–123

[20] Pan J. Y., Lin P., Maseeh F., Senturia S. D. 1990 Verification of FEM analysis of load-deflection methods for measuring mechanical properties of thin films, Tech. Digest IEEE Solid-State Sensor and Actuator Workshop 70–73

[21] Proost J. and Spaepen F. 2002 Evolution of the growth stress, stiffness, and microstructure of alumina thin films during vapor deposition J. Appl. Phys. **91** 204–216

[22] Miller D. C., Foster R. R., Jen H. S., Bertrand J. A., Cunningham S. J., Morris A. S., Lee Y. C., George S. M. and Dunn M. L. 2010 Thermo-mechanical properties of alumina films created using the atomic layer deposition technique Sens. Actuators, A **164** 58–67

[23] Borrero-Lopez O. and Hoffman M. 2014 Measurement of fracture strength in brittle films Surf. Coat. Technol. **254** 1–10

[24] SFS-EN 843-5 Advanced technical ceramics. Mechanical properties of monolithic ceramics at room temperature. Part 5: Statistical Analysis, Finnish Standards Association, 2007

[25] Murthy D. N. P., Xie M., Jiang R. 2004 Weibull Models Hoboken New Jersey Wiley 160–161

[26] Dingemans G., Einsele F., Beyer W., van den Sanden M. C. M., Kessels W. M. M. 2012 Influence of annealing and Al_2O_3 properties on the hydrogen-induced passivation of the Si/SiO_2 interface J. Appl. Phys. **111** 093713

[27] Lärmer F., Franssila S., Sainiemi L., Kolari K., 2015 Deep reactive ion etching in Part IV Micromachining technologies in MEMS edited by Franssila S. in Handbook of silicon based MEMS materials and technologies 2nd edition London Elsevier 444–469

[28] Davis J. R., Chapter 2 Mechanical Behavior of Materials under Tensile Loads in Tensile Testing, Geauga County, ASM International, 2004

[29] Wang L., Travis J. J., Cavanagh A. S., Liu X., Koenig S. P., Huang P. Y., George S. M., Bunch J. S. 2012 Ultrathin oxide films by atomic layer deposition on graphene Nano Lett. **12** 3706–3710

[30] Yuan F. and Huang L. 2012 Molecular dynamics simulation of amorphous silica under uniaxial tension: From bulk to nanowire J. Non-Cryst. Solids **358** 3481–3487

[31] Chowdhury S. C., Haque B. Z., Gillespie Jr. J. W. 2016 Molecular dynamics simulations of the structure and mechanical properties of silica glass using ReaxFF J. Mater. Sci. **51** 10139–10159

[32] Proctor B. A., Wihtney I., Johnson J. W. 1966 The strength of fused silica Proc. R. Soc. London Ser. A **297** 534–557

[33] Luo J., Wang J., Bitzek E., Huang J. Y., Zheng H., Tong L., Yang Q., Li J., Mao S. X. 2016 Size-dependent brittle-to-ductile transition in silica glass nanofibers Nano Lett. **16** 105–113